Safety Issues for Cardiac MR at (Ultra)high Fields: Physics and More

Thoralf Niendorf[1,2]

[1)] Berlin Ultrahigh Field Facility (B.U.F.F.), Max-Delbrueck Center for Molecular Medicine, Berlin, Germany
[2)] Experimental and Clinical Research Center (ECRC), Charité Campus Buch, Humboldt-University, Berlin, Germany

Introduction

A growing number of reports eloquently speak about explorations into cardiovascular MR (CVMR) at high (B_0=3.0T) and ultrahigh magnetic field strengths (B_0≥7.0T), with the goal of making the transition to the clinic. Realizing the opportunities and challenges of (ultra)high field CVMR in equal measure this presentation outlines UHF-MR physics together with safety issues at ultrahigh fields. The review is also an attempt to inspire the imaging community to throw further weight behind the solution of the many remaining challenges [1,2]. For this purpose MR safety considerations - including static magnetic fields, time varying and spatially varying magnetic fields, RF fields, implants and devices, and auxiliary hardware are surveyed. Of course, UHF-CVMR is an area of vigorous ongoing research, and many potentially valuable developments that tackle UHF-MR safety issues will receive only brief mention here.

Static Magnetic Fields (B_0)

MR at 7.0 T falls into the controlled operating mode category on static magnetic field limits recommended by the International Commission on Non-Ionizing Radiation Protection (ICNIRP) [3]. Repeated exposure to 7.0 T did not appear to affect neurogenesis, cell death or memory function in late gestation or in young postnatal rats [4]. Human studies showed no significant neurocognitive effects at 7.0 T. MRI examinations at 7.0 T do not seem to have any persisting influence on the attention networks of human cognition immediately after exposure [5]. A large scale study (n=573) revealed that 7 T MRI was perceived more uncomfortable than 1.5 T with significant differences regarding vertigo and sweating between 7 and 1.5 T [6]. The authors concluded that although certain sensations increase at 7 T compared to 1.5 T, they are unlikely to hinder the use of 7 T MRI as a clinical diagnostic tool [6]. Chakeres et. al. reported no clinically significant changes in the subjects' physiologic measurements at B_0=8.0 T, though a slight increase in the systolic blood pressure was found with increasing magnetic field strength [7]. Exposure to a 9.4T static magnetic field did not result in a statistically significant change in vital signs or cognitive ability of healthy volunteers [8].

Time Varying and Spatially Varying Magnetic Fields (dB/dt)

Thresholds for motion-induced vertigo have been estimated to be around 1 T s^{-1} for greater than 1 s [3]. Avoiding these sensations is likely to afford protection against other effects of induced electric fields and currents that arise as a consequence of motion in a static magnetic field [3]. Consequently, researchers, healthcare workers, volunteers and patients are asked to walk slowly in a UHF-MR environment in order not to exceed the limits for induced electric fields and current densities with the ultimate goal to reduce if not avoid the possibility of vertigo and nausea [3]. This translates into a recommendation derived from numerical simulations that a walking speed of 1 m s^{-1} should not be exceeded when accessing an area closer than 2 m to the front ends of a 7.0 T magnet [9]. For the same reason there is a need to ensure that subjects are moved slowly into the 7.0 T magnet bore. It is highly recommended that patient table motion is set to be lower than 1 T s^{-1}. To meet this requirement a feature which sets the table motion to be inverse proportional to the gradient in the magnetic field strength is offered by some vendors.

Magnetic Fringe Fields

Magnetic forces of fringe magnetic fields of MR systems on ferromagnetic components can impose a severe patient, occupational health and safety hazard. MRI accidents are listed as number 9 of the top 10 risks in modern medicine [10,11]. With the advent of (ultra)high field MR systems [1,12-22] this risk, which is commonly known as the missile or projectile effect is even more pronounced. At ultrahigh fields fringe fields are largely increased as illustrated in Figure 1. Most MRI accidents occur when non-MRI personnel (or careless MRI workers) introduce ferromagnetic objects into the magnetic environment [23]. It is estimated that the reported incidents only account for about 10% of the actual number of such incidents, and even in this case, the number of incidents has jumped approximately 300% from 2004 to 2008 [24,25]. Various policies [26-29] have been implemented to safeguard healthcare workers, volunteers and patients with the ultimate goal of avoiding unforeseen disasters and injuries due to ferromagnetic objects**.** These measures safety initiatives and awareness campaigns spearheaded by scientific organizations and other bodies and include safety training, risk reduction strategies, occupational health instructions, safety guidelines and warning signs. These safety procedures are commonly supplemented by metal or ferromagnetic detectors which are positioned at the entrance of the MR scanner room for example, as well as hall sensors [30] and other magnetic field sensing devices. The costs of traditional metal or ferromagnetic detectors are significant. Stand alone detector configurations and handheld scanners are frequently not properly used due to the heavy work load as well as busy environment experienced by hospital staff. Furthermore, some detectors used in current clinical practice do not distinguish between ferromagnetic and non- ferromagnetic objects, thus making it difficult for hospital staff to maintain MR safety. Warning labels on the doors, walls or on the ground denoting the 5 G and 10 G are likely to be overlooked in a fast paced hospital environment. Thus auditory or visual warning of ferromagnetic objects being brought into the MR environment is necessary. A strategy employing small magnetic field alert sensors which can be attached to ferromagnetic objects that are commonly used in a clinical environment is conceptually appealing for the pursuit of reducing the risk of ferromagnetic projectile accidents. Recently a simple, cost-effective and mobile *m*agneto *al*ert *se*nsor (MALSE) which provides alarm in the presence of static magnetic fields and which can be used in various configurations was proposed [31]. MALSE is a simple concept for alerting MRI staff to a ferromagnetic object being brought into fringe magnetic fields which exceeds MALSEs activation magnetic field as demonstrated in Figure 1. MALSE can easily be attached to ferromagnetic objects within the vicinity of a scanner, thus creating a barrier for hazardous situations induced by ferromagnetic parts which should not enter the vicinity of a MR-system to occur.

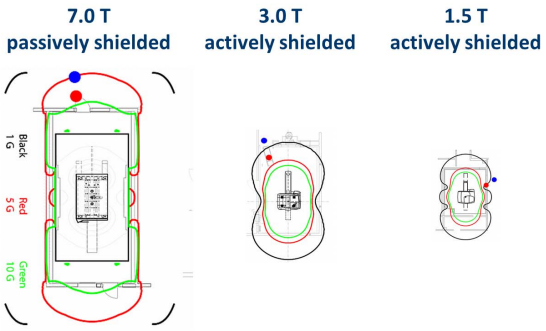

Figure 1: Schematics of the fringe field of a passively shielded 7.0 T **(left)**, an actively shielded 3.0 T **(middle)** and an actively shielded 1.5 T **(right)** MR system. The 10 G, 5 G and 1 G lines are marked in green, red and black , starting from the magnet's iso-center. The position at which a small and mobile magneto alert sensor MALSE got activated is marked in red.

RF Fields

RF energy can induce a heating effect. Since it is difficult to measure internal temperature changes RF heating must be evaluated carefully by the assessment of the specific absorption rate (SAR), which scales with B_0^2. For the assessment of B_1^+ distribution and RF safety purpose numerical electromagnetic field (EMF) simulations must be performed. Power settings of RF coils need to be based on careful examinations of the partial body and local SAR values according to the IEC guidelines [32]. An example of EMF simulations for local TX/RX coils tailored for cardiac MR at 7.0 T is shown in Figure 2 [33].

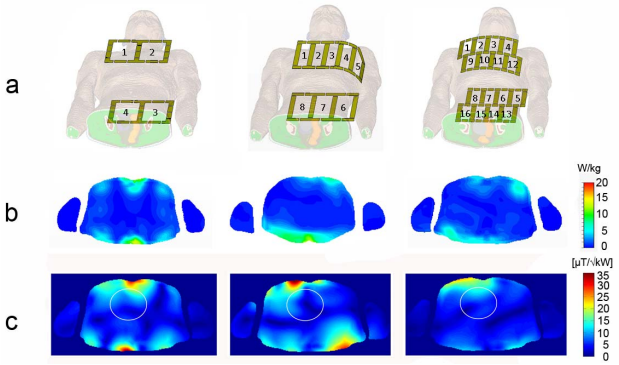

Figure 2: (a) Basic schemes of the three TX/RX coil designs tailored for cardiac MR at 7.0 T: **left)** 4-channel TX/RX coil with two anterior and two posterior elements of size (13x20)cm^2 (S-I dimension: 20cm; L-R dimension: 26cm) (12), **center)** 8-channel TX/RX coil with five anterior elements each with a size of (6x19)cm^2 plus three posterior elements with a size of (9x19)cm^2 (S-I dimension: 21cm; L-R dimension: 31cm), **right)** 16-channel TX/RX coil with eight anterior and eight posterior elements with a size of (6x13)cm^2 (S-I dimension: 28cm; L-R dimension: 29cm). **(b)** Simulation of the signal-absorption rate (SAR) distribution (local SAR, 10g average) for an axial slice for the 4 (**left**), 8 (**middle**) and 16 (**right**) channel TX/RX coil. The limits for partial body SAR or for maximum local SAR of 20W/kg given by the IEC (13) were not exceeded. **(c)** Simulation of the transmit field efficiency ($B_1^+/\sqrt{P_{delivered}}$) in a mid-axial view of the 4 (**left**), 8 (**middle**) and 16 (**right**) channel TX/RX coil. The white colored ROI indicates the position of the heart.

Constraints dictated by the physics of the applied RF fields at higher frequencies (≥ 300 MHz) constitute a significant challenge for ultrahigh field MR. The short wavelength of the RF fields inside the tissue (≈ 12 cm) and increased dielectric effects lead to highly complex and non-uniform B_1^+ distributions [34,35] causing shading or local signal drop-off but also local B_1^+ and SAR hot spots. This behavior has inspired explorations into novel radiofrequency (RF) technology including multichannel transmit/receive (TX/RX) technology [36-39] including various coil multi transmit coil designs tailored for cardiac and body MR at 7.0 T [33,40-44]. This approach helps to overcome some of the transmit B_1^+ field heterogeneity and RF power deposition constraints present at ultrahigh fields by using B_1^+ shimming [45,46]. B_1^+ shimming is a special case of parallel transmission in which the driving amplitude and phase are adjusted at multiple transmit ports or coils in order to tailor excitation patterns. B_1^+ shimming is typically used to reduce RF non-uniformities and to maximize B_1^+ coherence as illustrated in Figure 3. B_1^+ shimming can be also put to use to enhance the excitation efficiency or to relax RF power deposition as outlined in Figure 3. The supervision of local specific absorption rate (SAR) in parallel transmission applications using EMF simulations is essential but remains challenging. Practical challenges arise for the adequate handling and comparing of pre-calculated field distributions as long as the expected combined radiofrequency excitations are still undetermined [47]. To solve this problem several methods were proposed to significantly reduce the complexity without restriction to particular radiofrequency excitations [47-51]. In a particular implementation it was demonstrated that by constructing several matrices it is sufficient to consider only so-called Virtual Observation Points for an adequate, conservative estimation of the maximum local SAR [47].

Although SAR is key for RF safety evaluations it should be noted that the temperature distribution - which is the cause of tissue damage based on RF heating - doesn't follow SAR in a straightforward manner [52]. Thermoregulation and heat transfer inside the body (i.e. blood vessels) need to be considered while moving towards a more realistic scenario. Here ongoing research focusses already on temperature modeling instead of SAR models, suggesting a thermal tissue damage threshold CEM43 known from thermal therapies [53,54]. These explorations will help to advance towards enhanced MR safety assessment for CVMR at high and ultrahigh fields. While the technical details of characterizing SAR and temperature are being perfected, methods for interpreting the results of these calculations in the light of regulatory limits also warrant discussion [52]. Numerical simulations showed that the ratio of maximum local SAR to whole body average SAR did exceed regulatory limits by a significant factor when using whole body volume coil configurations at 1.5T and 3T [52]. This implies that today's UHF-CVMR operates at more conservative assumptions than widely used for CVMR at the lower fields. To summarize, RF power deposition constraints pose significant challenges for UHF CMR. This makes some CMR applications which are clinical routine at lower fields - for example steady state free precession (SSFP) imaging and fast spin echo imaging – elusive at ultrahigh fields yet. What might appear to be an enigma at the first glance can be deciphered by further explorations into the physics and physiology of RF induced heating.

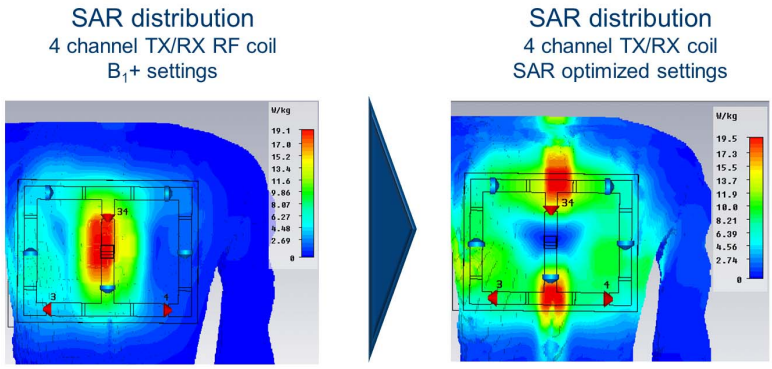

Figure 3: Signal absorption rate (SAR) simulations which demonstrate the impact of B_1^+ shimming on SAR in a human voxel model. For this purpose a 4 channel transmit/receive cardiac RF coil was used. Point SAR simulations of the cardiac coil: **left)** with B_1^+ being tailored to improve B_1^+ uniformity across the heart and **right)** B_1^+ being customized for SAR reduction without diminishing B_1^+ uniformity across the heart severely.

Radiofreqency Heating Induced by Implants, Devices and Intracoronary Stents

The presence of conducting objects in combination with RF wave lengths and RF power deposition used at (ultra)high fields may induce local RF heating which might cause tissue damage. It should be noted that the short wavelength of the RF fields inside tissue at 7.0 T is approximately 12 cm and hence can fall into the same range as the length of implants, stents or cardiac assist devices. For all these reasons it is essential to carefully assess RF induced heating in cardiac assist devices, implants and coronary stents.

Intracoronary stents commonly used in percutaneous interventions - a revascularization procedure for treatment of acute and chronic coronary artery disease (CAD) - are currently considered to be contra-indications for UHF-CVMR due to the relative lack of data describing the interference between conductive implants and EMF. Arguably, the notion that intracoronary stents are a contra-indication *per se* at 7.0 T is somewhat premature, as is an *a priori* statement which declares stents to be safe at 7.0 T. However, gaining a better insight into the MR safety of stents is of profound relevance for UHF-CMR developments and their transfer into clinical practice due to an increasing patient

population with a history of percutaneous coronary interventions (PCI) and stent implementation [55] with PCI rates increasing about 128% for the period 1987-2001, with an average increase of 6% per year for a selected population [56] and with 91% of coronary angiography interventions leading to stent implementation [55,56]. *A priori*, it cannot be ruled out that the antenna effect due to the presence of conducting implants in conjunction with the decrease in RF wave lengths and the increase in RF energy may bear the potential to cause RF power deposition at ultrahigh fields that may induce local heating and may potentially cause myocardial tissue damage and may influence coagulation or affect endothelial function.

With special attention to guidelines of the International Commission on Non-Ionizing Radiation Protection (ICNIRP) [57] and its implications for cardiac MRI at 7.0 T interference between copper tubes or coronary stents and *E*-field distribution was recently carefully examined using numerical simulations [58]. For this purpose a copper tube and a CAD model of a stent (PRO-Kinetic Energy Cobalt Chromium Coronary Stent System, Biotronik, Bülach, CH, l=40 mm, d= 4mm) were used together with an electric dipole excitation. The copper tube and the stent were positioned parallel to the electric field vector radiated by the dipole antenna. To scrutinize subtle details of the *E*-field distribution along the complex structure of the stent high resolution EMF simulations using a mesh size of (60×60×60) μm^3 for regions inside and in close vicinity of the devices were performed. The copper tube provided a reasonable approximation of a coronary stent [58] since its antenna effect is similar to that of a coronary stent. The *E*-field distribution derived for the copper tube and the stent are similar at a scale distance larger than $d/2$, where d is the diameter of the device. At smaller scales, the structure of the stent induces smaller variations of the *E*-field which however never exceed the value at the tips. The maximum *E*-field at the tips of the stent is approximately 25% higher than that of the copper tube, where the *E*-field is more homogeneously distributed along the circular edge. The coronary stents showed an RF heating behavior similar to that of a copper tube with the same geometry [58]. Unlike the copper tube stents present a network structure in which local hotspots could be present due to parasitic capacitances. Unfortunately MR thermometry is not capable to provide information within the stent network due to the MR artifacts induced by the stent. Here high spatial resolution EMF simulations hold the promise to provide a better insight into the RF heating pattern inside of a stent.

In addition to EMF simulations RF heating experiments were conducted at 7.0 T [58,59]. For this purpose a copper tube and coronary stents were embedded in agarose phantoms with electromagnetic properties that mimic myocardium. A highpass circular polarized birdcage RF coil that is capable of irradiating RF power to exceed the SAR limits defined by the IEC 60601-2-33 standard by factor ≈3. The temperature changes induced by RF heating over a one hour period at these high RF power levels reached approximately ΔT =27 K in the reference phantom. The extra temperature increase due to the presence of the copper tube or the coronary stents did not exceed 3 K which is within the experimental error of MR thermometry T [58,59].

The EMF simulations and RF heating experiments reported hitherto suggest that if IEC standards for local and global SAR limits are strictly obeyed, the extra RF heating, induced in myocardial tissue due to the presence of stents, may not be significant versus the baseline heating induced by a cardiac optimized transmit RF coil at 7.0 T [58]. In this context a recent study included a broad portfolio of clinical stent configurations into heating experiments [60]. None of the twenty clinical peripheral stent grafts (for a detailed list of devices included in this study please see [60]) produced a temperature rise of ≥ 2K even though permissible SAR limits were exceeded substantially [60]. Based on these results the authors conclude that RF heating of implanted stents is not a safety issue for UHF-MR. While these preliminary results are encouraging further research will include careful investigation of stent configurations which involve multiple stents with different size,

geometry and design, a configuration which is very common in patients with history of percutaneous interventions.

To summarize, the MR-safety assessment of implants, intracoronary stents and other implantable medical devices at 7.0 T is at a very early exploration stage. Further careful investigations are required before intracoronary stents pace makers, mitral and aortic valve replacements, cochlear implants, insulin pumps, neuro-stimulators and other implantable medical devices can be declared to be MR safe in a UHF-MR environment and hence remain contra-indications for UHF-MR, unless otherwise stated, certified or approved for UHF-MR.

Auxiliary Hardware

As ultrahigh-field MRI becomes more widespread, the significance of artifact sensitivity of ECG recordings increases and with it the motivation for a practical gating/triggering alternative. Since ECG is an inherently electrical measurement with electrically active components [61], it does carry a risk of surface heating of patients' skin and even of severe skin burns resulting from induction of high voltages in ECG hardware [28,62-65]. The FDA's MAUDE data base reports several skin burns in the last 5 years due to induction of high voltages in ECG hardware due to interaction with RF signals [23]. The use of non MR safe ECG hardware has even caused an incident in the MR bore, where high-voltage induction in ECG wiring caused a fire[62]. Various technologies have been implemented on clinical scanners to safeguard patients with the ultimate goal of avoiding disasters and injuries due to ECG hardware**.** These measures involve the use of (i) ECG electrodes being classified as MR-safe, (ii) ECG leads shorter than the RF wave length and (iii) high impedance leads, fiber optic leads or wireless connections for signal transfer. Consequently, user manuals of clinical scanners outline explicitly that MR-safe electrodes which are made available through the MR vendor's accessories catalogue must be used. Also, the manufacturer's user manuals for RF coils advice to use extra padding for keeping RF coils in a safe distance from the chest as illustrated in Figure 4. This measure has been implemented to avoid ECG electrodes being positioned in areas close to local signal absorption rate (SAR) hot spots caused by the RF coil's EM fields. For further details please feel free to download a book chapter on ECG in an MR environment from: http://www.intechopen.com/books/advances-in-electrocardiograms-methods-and-analysis/electrocardiogram-in-an-mri-environment-clinical-needs-practical-considerations-safety-implications-

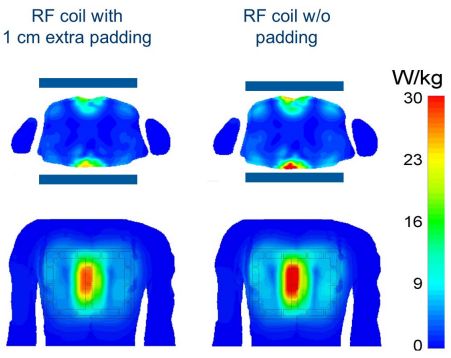

Figure 4: Axial and coronal views of the upper torso derived from signal absorption rate (SAR_{10g}) simulations The simulations demonstrate the impact of extra padding for the purpose of keeping RF coils in a safe distance from ECG electrodes. For padding an extra layer with a thickness of 1c m was inserted between the anterior and posterior section of the coil and the anterior and posterior upper chest. For the simulations a 4 channel transmit/receive RF cardiac coil was used together with an accepted power of 30 W without padding (left) and with padding (right). With padding a maximum local SAR_{10g} value of 18.1 W/kg is reached. Without padding the maximum local SAR_{10g} value increased to 21.2 W/kg. This value would exceed the IEC safety guidelines of 20 W/kg.

ECG and even advanced vector-cardiogram (VCG, [66]) approaches are corrupted by interference from electromagnetic fields and by magneto-hydrodynamic effects which increase with increasing magnetic field strengths [67]. Consequently, artifacts in the ECG/VCG trace and T-wave elevation might be mis-interpreted as R-waves, resulting in erroneous triggering together with motion corrupted image quality, an issue which is pronounced at ultrahigh fields. For all of these reasons, a non-invasive acoustic cardiac triggering (ACT) approach (which may also be termed "MR stethoscopy") was recently proposed in the pursuit of reliable cardiac gating [68], as illustrated schematically in Figure 5. ACT does not require any hardware or software changes on the scanner side and ensures full compliance with safety regulations for medical devices. The MR-stethoscope presents no risk of high voltage induction and patient burns, suitability for a broad range of magnetic field strengths, patient comfort, ease of clinical use, insensitivity to electromagnetic fields and high trigger reliability. Acoustic cardiac gating was found to meet the demands of cardiac MR applications at 1.5 T, 3.0 T and 7.0 T, including breath-hold and free-breathing acquisition strategies together with prospective and retrospective triggering regimes [69,70].

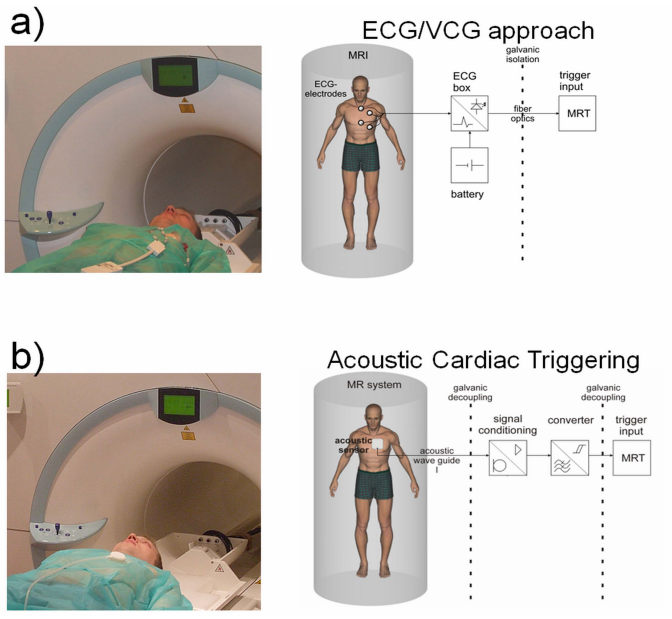

Figure 5: Clinical setup **(left)**, block diagram **(right)** for **a)** conventional ECG gating and **b)** acoustic cardiac triggering (ACT) for synchronization of MR imaging with the cardiac cycle. Note that neither the limited ECG in the MR scanner nor the acoustic waveforms obtained for acoustic cardiac gating should be treated as reliable indicators of patient emergency conditions.

Acknowledgement

The author gratefully acknowledges the enthusiastic and energetic members of the Berlin Ultrahigh Field Facility (B.U.F.F.), Berlin, Germany whom kindly contributed examples of their pioneering work or other valuable assistance.

References

1. Niendorf T, Sodickson DK, Krombach GA, Schulz-Menger J (2010) Toward cardiovascular MRI at 7 T: clinical needs, technical solutions and research promises. Eur Radiol 20: 2806-2816.
2. Niendorf T, Graessl A, Thalhammer C, Dieringer MA, Kraus O, et al. (2013) Progress and promises of human cardiac magnetic resonance at ultrahigh fields: a physics perspective. J Magn Reson 229: 208-222.

3. ICNIRP (2009) Amendment to the ICNIRP "Statement on Medical Magnetic Resonance (MR) Procedures: Protection of Patients". Health Physics 97: 259-261.
4. Zhu C, Gao J, Li Q, Huang Z, Zhang Y, et al. (2011) Repeated exposure of the developing rat brain to magnetic resonance imaging did not affect neurogenesis, cell death or memory function. Biochem Biophys Res Commun 404: 291-296.
5. Schlamann M, Voigt MA, Maderwald S, Bitz AK, Kraff O, et al. (2010) Exposure to high-field MRI does not affect cognitive function. J Magn Reson Imaging 31: 1061-1066.
6. Heilmaier C, Theysohn JM, Maderwald S, Kraff O, Ladd ME, et al. (2011) A large-scale study on subjective perception of discomfort during 7 and 1.5 T MRI examinations. Bioelectromagnetics.
7. Chakeres DW, de Vocht F (2005) Static magnetic field effects on human subjects related to magnetic resonance imaging systems. Prog Biophys Mol Biol 87: 255-265.
8. Atkinson IC, Renteria L, Burd H, Pliskin NH, Thulborn KR (2007) Safety of human MRI at static fields above the FDA 8 T guideline: sodium imaging at 9.4 T does not affect vital signs or cognitive ability. J Magn Reson Imaging 26: 1222-1227.
9. Crozier S, Wang H, Trakic A, Liu F (2007) Exposure of workers to pulsed gradients in MRI. J Magn Reson Imaging 26: 1236-1254.
10. Legge A (2009) A review of the top 10 health technology hazards and how to minimise their risks. Nurs Times 105: 17-19.
11. ECRI (2008) Top 10 health technology hazards. Health Devices 37: 343-350.
12. Robitaille PM, Abduljalil AM, Kangarlu A, Zhang X, Yu Y, et al. (1998) Human magnetic resonance imaging at 8 T. NMR Biomed 11: 263-265.
13. Vaughan T, DelaBarre L, Snyder C, Tian J, Akgun C, et al. (2006) 9.4T human MRI: preliminary results. Magn Reson Med 56: 1274-1282.
14. Barth M, Meyer H, Kannengiesser SA, Polimeni JR, Wald LL, et al. (2010) T2-weighted 3D fMRI using S2-SSFP at 7 tesla. Magn Reson Med 63: 1015-1020.
15. Tallantyre EC, Morgan PS, Dixon JE, Al-Radaideh A, Brookes MJ, et al. (2009) A comparison of 3T and 7T in the detection of small parenchymal veins within MS lesions. Invest Radiol 44: 491-494.
16. Vaughan JT, Snyder CJ, DelaBarre LJ, Bolan PJ, Tian J, et al. (2009) Whole-body imaging at 7T: preliminary results. Magn Reson Med 61: 244-248.
17. Umutlu L, Maderwald S, Kraff O, Theysohn JM, Kuemmel S, et al. (2010) Dynamic contrast-enhanced breast MRI at 7 Tesla utilizing a single-loop coil: a feasibility trial. Acad Radiol 17: 1050-1056.
18. Umutlu L, Orzada S, Kinner S, Maderwald S, Brote I, et al. (2011) Renal imaging at 7 Tesla: preliminary results. Eur Radiol 21: 841-849.
19. van Elderen SG, Versluis MJ, Westenberg JJ, Agarwal H, Smith NB, et al. (2010) Right coronary MR angiography at 7 T: a direct quantitative and qualitative comparison with 3 T in young healthy volunteers. Radiology 257: 254-259.
20. von Knobelsdorff-Brenkenhoff F, Frauenrath T, Prothmann M, Dieringer MA, Hezel F, et al. (2010) Cardiac chamber quantification using magnetic resonance imaging at 7 Tesla-a pilot study. Eur Radiol 20: 2844-2852.
21. Frauenrath T, Hezel F, Renz W, de Geyer TdO, Dieringer M, et al. (2010) Acoustic cardiac triggering: a practical solution for synchronization and gating of cardiovascular magnetic resonance at 7 Tesla. J Cardiovasc Magn Reson 12: 67.
22. Dieringer M, Renz W, Lindel T, Seifert F, Frauenrath T, et al. (2011) Design and Application of a Four-Channel Transmit/Receive Surface Coil for Functional Cardiac Imaging at 7T. J Magn Reson Imaging epub ahaead of print.
23. Health USFaDACfDaR (2010) MAUDE data base reports of adverse events involving medical devices. U.S. Food and Drug Administration. Center for Devices and Radiological Health.
24. Yee KM (2009) Rise in MRI accidents highlights need for magnet safety. Auntminnie Web site.
25. Gilk T (2009) Risky Business: MRI accidents increase fourfold in as many years. image the source for radiology professionals.
26. Kanal E, Barkovich AJ, Bell C, Borgstede JP, Bradley WG, Jr., et al. (2007) ACR guidance document for safe MR practices: 2007. AJR Am J Roentgenol 188: 1447-1474.
27. Administration USFaD (2009) A Primer on Medical Device Interactions with Magnetic Resonance Imaging Systems. U.S. Food and Drug Administration.

28. Shellock FG, Crues JV (2004) MR procedures: biologic effects, safety, and patient care. Radiology 232: 635-652.
29. Shellock FG, Woods TO, Crues JV, 3rd (2009) MR labeling information for implants and devices: explanation of terminology. Radiology 253: 26-30.
30. Molyneaux DA, Ceisla J, Tsalikis D (2009) Method and Apparatus for Ferrous Object and/or Magnetic Field Detection for MRI Safety United States: Koninklijke Philips Electronics N.V. (BA Eindhoven, NL)
31. Martin C, Frauenrath T, Ozerdem C, Renz W, Niendorf T (2011) Development and evaluation of a small and mobile Magneto Alert Sensor (MALSE) to support safety requirements for magnetic resonance imaging. Eur Radiol 21: 2187-2192.
32. IEC (2010) 60601-2-33 Medical electrical equipment - Part 2-33: Particular requirements for the basic safety and essential performance of magnetic resonance equipment for medical diagnosis. Edition 3.0.
33. Winter L, Kellman P, Renz W, Grassl A, Hezel F, et al. (2012) Comparison of three multichannel transmit/receive radiofrequency coil configurations for anatomic and functional cardiac MRI at 7.0T: implications for clinical imaging. Eur Radiol.
34. Van de Moortele PF, Akgun C, Adriany G, Moeller S, Ritter J, et al. (2005) B1 destructive interferences and spatial phase patterns at 7 T with a head transceiver array coil. Magn Reson Med 54: 1503-1518.
35. Yang QX, Wang J, Zhang X, Collins CM, Smith MB, et al. (2002) Analysis of wave behavior in lossy dielectric samples at high field. Magn Reson Med 47: 982-989.
36. Katscher U, Bornert P (2006) Parallel RF transmission in MRI. NMR Biomed 19: 393-400.
37. Katscher U, Bornert P, Leussler C, van den Brink JS (2003) Transmit SENSE. Magn Reson Med 49: 144-150.
38. Zhu Y (2004) Parallel excitation with an array of transmit coils. Magn Reson Med 51: 775-784.
39. Ullmann P, Junge S, Wick M, Seifert F, Ruhm W, et al. (2005) Experimental analysis of parallel excitation using dedicated coil setups and simultaneous RF transmission on multiple channels. Magn Reson Med 54: 994-1001.
40. Vaughan JT, Snyder CJ, DelaBarre LJ, Bolan PJ, Tian J, et al. (2009) Whole-body imaging at 7T: preliminary results. Magn Reson Med 61: 244-248.
41. Snyder CJ, DelaBarre L, Metzger GJ, van de Moortele PF, Akgun C, et al. (2009) Initial results of cardiac imaging at 7 Tesla. Magn Reson Med 61: 517-524.
42. Dieringer MA, Renz W, Lindel T, Seifert F, Frauenrath T, et al. (2011) Design and application of a four-channel transmit/receive surface coil for functional cardiac imaging at 7T. J Magn Reson 33: 736-741.
43. Grassl A, Winter L, Thalhammer C, Renz W, Kellman P, et al. (2011) Design, evaluation and application of an eight channel transmit/receive coil array for cardiac MRI at 7.0T. Eur J Radiol.
44. Thalhammer C, Renz W, Winter L, Hezel F, Rieger J, et al. (2012) Two-Dimensional sixteen channel transmit/receive coil array for cardiac MRI at 7.0 T: Design, evaluation, and application. J Magn Reson Imaging.
45. Van de Moortele PF, Akgun C, Adriany G, Moeller S, Ritter J, et al. (2005) B(1) destructive interferences and spatial phase patterns at 7 T with a head transceiver array coil. Magn Reson Med 54: 1503-1518.
46. Vaughan JT, Adriany G, Snyder CJ, Tian J, Thiel T, et al. (2004) Efficient high-frequency body coil for high-field MRI. Magn Reson Med 52: 851-859.
47. Eichfelder G, Gebhardt M (2011) Local specific absorption rate control for parallel transmission by virtual observation points. Magn Reson Med 66: 1468-1476.
48. Wolf S, Diehl D, Gebhardt M, Mallow J, Speck O (2012) SAR simulations for high-field MRI: How much detail, effort, and accuracy is needed? Magn Reson Med.
49. Graesslin I, Homann H, Biederer S, Bornert P, Nehrke K, et al. (2012) A specific absorption rate prediction concept for parallel transmission MR. Magn Reson Med.
50. Homann H, Graesslin I, Eggers H, Nehrke K, Vernickel P, et al. (2012) Local SAR management by RF Shimming: a simulation study with multiple human body models. MAGMA 25: 193-204.
51. Homann H, Bornert P, Eggers H, Nehrke K, Dossel O, et al. (2011) Toward individualized SAR models and in vivo validation. Magn Reson Med 66: 1767-1776.

52. Wang Z, Lin JC, Mao W, Liu W, Smith MB, et al. (2007) SAR and temperature: simulations and comparison to regulatory limits for MRI. Journal of Magnetic Resonance Imaging 26: 437-441.
53. Murbach M, Neufeld E, Pruessmann KP, Kuster N (2012) Safe MR scan times based on CEM43 tissue damage thresholds, using electromagnetic and thermal simulations with anatomically correct human models and considering local thermoregulation. Proc Intl Soc Mag Reson Med.
54. Yarmolenko PS, Moon EJ, Landon C, Manzoor A, Hochman DW, et al. (2011) Thresholds for thermal damage to normal tissues: An update. International Journal of Hyperthermia 27: 320-343.
55. Rawson NS, Chu R, Ismaila AS, Terres JA (2012) The aging Canadian population and hospitalizations for acute myocardial infarction: projection to 2020. BMC Cardiovasc Disord 12: 25.
56. Ulrich MR, Brock DM, Ziskind AA (2003) Analysis of trends in coronary artery bypass grafting and percutaneous coronary intervention rates in Washington state from 1987 to 2001. Am J Cardiol 92: 836-839.
57. (2004) ICNIRP Statement on medical magnetic resonance (MR) procedures: protection of patients. HEALTH PHYSICS 87: 20
58. Santoro D, Winter L, Mueller A, Vogt JM, Renz W, et al. (2012) Detailing Radio Frequency Heating Induced by Coronary Stents: A 7.0 Tesla Magnetic Resonance Study. PloS ONE 7: e49963.
59. Santoro D, Müller A, Winter L, Renz W, Gräßl A, et al. Analysis of radio frequency heating induced by a coronary stent at 7.0T; 2012.
60. Ansems J, Kolk A, Kroeze H, Van den Berg NAT, Borst G, et al. MR Imaging of Patients with Stents is Safe at 7.0 Tesla; 2012. pp. 2764.
61. Lanzer P, Barta C, Botvinick EH, Wiesendanger HU, Modin G, et al. (1985) ECG-synchronized cardiac MR imaging: method and evaluation. Radiology 155: 681-686.
62. Kugel H, Bremer C, Puschel M, Fischbach R, Lenzen H, et al. (2003) Hazardous situation in the MR bore: induction in ECG leads causes fire. Eur Radiol 13: 690-694.
63. Shellock FG, Kanal E (1996) Burns associated with the use of monitoring equipment during MR procedures. J Magn Reson Imaging 6: 271-272.
64. Stralka JP, Bottomley PA (2007) A prototype RF dosimeter for independent measurement of the average specific absorption rate (SAR) during MRI. J Magn Reson Imaging 26: 1296-1302.
65. Stecco A, Saponaro A, Carriero A (2007) Patient safety issues in magnetic resonance imaging: state of the art. Radiol Med 112: 491-508.
66. Fischer SE, Wickline SA, Lorenz CH (1999) Novel real-time R-wave detection algorithm based on the vectorcardiogram for accurate gated magnetic resonance acquisitions. Magn Reson Med 42: 361-370.
67. Stuber M, Botnar RM, Fischer SE, Lamerichs R, Smink J, et al. (2002) Preliminary report on in vivo coronary MRA at 3 Tesla in humans. Magn Reson Med 48: 425-429.
68. Frauenrath T, Niendorf T, Kob M (2008) Acoustic method for synchronization of Magnetic Resonance Imaging (MRI). Acta Acustica united with Acustica: 148-155.
69. Frauenrath T, Hezel F, Heinrichs U, Kozerke S, Utting JF, et al. (2009) Feasibility of cardiac gating free of interference with electro-magnetic fields at 1.5 Tesla, 3.0 Tesla and 7.0 Tesla using an MR-stethoscope. Invest Radiol 44: 539-547.
70. Becker M, Frauenrath T, Hezel F, Krombach GA, Kremer U, et al. (2010) Comparison of left ventricular function assessment using phonocardiogram- and electrocardiogram-triggered 2D SSFP CINE MR imaging at 1.5 T and 3.0 T. Eur Radiol 20: 1344-1355.